# Monte Carlo transport of swift protons and light ions in water: The influence of excitation cross sections, relativistic effects, and Auger electron emission in w-values

Verónica Belén Tessaro, Benoit Gervais, Floriane Poignant, Michael Beuve, Mariel Elisa Galassi

# Monte Carlo transport of swift protons and light ions in water: the influence of excitation cross sections, relativistic effects, and Auger electron emission in *w*-values

Verónica. Belén. Tessaro[1,2], Benoit. Gervais[3], Floriane. Poignant[12], Michael. Beuve[2] and Mariel Elisa Galassi[1]

[1]Grupo de Física Biomédica, Instituto de Física de Rosario (CONICET-UNR) and Facultad de Ciencias Exactas, Ingeniería y Agrimensura, Universidad Nacional de Rosario (UNR), C.P.2000 Rosario, Argentina.

[2]Université de Lyon, F-69622; Université de Lyon 1, CNRS/IN2P3, Institut de Physique des 2 Infinis de Lyon, Villeurbanne, France.

[3]Centre de Recherche sur les Ions, les Matériaux et la Photonique (UMR6252), CEA/CNRS/ENSICAEN/Université de Caen-Basse Normandie UCBN, CIMAP-CIRIL-Ganil, BP 5133, 14070, Cedex 05, Caen, France.

Corresponding author: V. B. Tessaro. verotessaro@gmail.com

## Abstract

*Purpose:* To develop a particle transport code to compute *w*-values and stopping power of swift ions in liquid water and gases of interest for reference dosimetry in hadrontherapy. To analyze the relevance of inelastic and post-collisional processes considered.

*Methods:* The Monte Carlo code MDM was extended to the case of swift ion impact on liquid water (MDM-Ion). Relativistic corrections in the inelastic cross sections and the post-collisional Auger emission were considered. The effects of introducing different electronic excitation cross sections were also studied.

*Results:* The stopping power of swift ions on liquid water, calculated with MDM-Ion, are in excellent agreement with recommended data. The *w*-values show a strong dependence on the electronic excitation cross sections and on the Auger electron emission. Comparisons with other Monte Carlo codes show the relevance of both the processes considered and of the cross sections employed. *W* and *w*-values for swift electron, proton, and carbon ions calculated with the MDM and MDM-Ion codes are in very close agreement with each other and with the 20,8 eV experimental value.

[1] Current address: National Institute of Aerospace, Hampton, VA, USA

*Conclusion:* We found that *w*-values in liquid water are independent of ion charge and energy, as assumed in reference dosimetry for hadrontherapy from sparse experimental results for electron and ion impact on gases. Excitation cross sections and Auger emission included in Monte Carlo codes are critical in *w*-values calculations. The computation of this physical parameter should be used as a benchmark for micro-dosimetry investigations, to assess the reliability of the cross sections employed.

Keywords: W-values, ions, dosimetry, stopping power, Auger emission

## 1. Introduction

Describing the effect of ionizing radiation in liquid water is mandatory to better understand its chemical and biological consequences, as water is the major constituent of biological tissues. To that end, it is necessary to model the physical interactions involved by the incident projectile as it passes through biological matter. Monte Carlo (MC) codes of particle transport are important computational tools that have the ability to simulate all these physical processes, tracking down to threshold energy both primary particles and all secondary electrons generated by ionization of target molecules (e.g., water molecules). Several simulation platforms have been developed so far and are still being extended to study the energy deposition in biomolecules and cells for ionizing projectiles in water [1–4]. The outcomes of such simulations may also be used to predict biological quantities, like cell survival fraction due to ion irradiations, relying on a realistic description of the spatial distribution of ionizations, excitations and also chemical species produced by water radiolysis [5–7]. Track structure codes are widely preferred since they provide a detailed treatment of all the interactions using scattering models that give an appropriate spatial resolution for small biological targets.

In this work, a new branch of the MDM code, called MDM-Ion, for ion projectiles in liquid water is presented. The original transport code MDM arises from the LQD code, which has the ability to track event-by-event electrons and ions in liquid water. LQD code was first developed to simulate the production of radical species by the interaction of swift heavy ions with liquid water [8]. It was then modified to contemplate various heterogeneous domains, which has led to the creation of a restructured version, MDM for MeDiuM, used to study the radiolysis of water confined in porous silica [9], or more recently to study the influence of gold nanoparticles in water on nano dosimetry and chemical species production [10–12] and physical parameters of relevance in reference dosimetry, *W*-values calculations [13]. Starting with liquid water as the target medium allows us to

compare with other MC codes as RETRACK [14], GEANT4-DNA [15], KURBUC [16], SEICS [17], or PARTRAC [3], among the most widely used codes for radiation biology and recommended data.

One of the main goals in making the MDM-Ion branch code to ion projectiles was to study physical parameters of relevance in ion radiation therapy (called protontherapy for swift protons and hadrontherapy for carbon and other light ions). To provide a precise dose delivery to the patients, the reference dosimetry must be accurately determined. There are several international protocols that provide a methodology to determine the absorbed dose in liquid water. The TRS-398 [18] is one of them and is currently used for hadrontherapy. It describes a procedure to determine the absorbed dose in liquid water using ionization chambers filled with air. To obtain the absorbed dose from the dosimeter reading, conversion factors are needed. Among them, the stopping power ratio of liquid water to air and the *w*-values in air are the ones that contribute the most to uncertainties in the dose determination [18,19].

The *W*-value is defined as the mean energy required to form an ion-electron pair after the complete dissipation of the projectile initial energy. In the case of swift proton and light ion beams used in hadrontherapy, they lose only a fraction of their energy when traversing the gas volume of the ionization chamber. Therefore, the proper conversion coefficient to be used is the differential value, *w*. It has been observed for electron beams that values of *w* and *W* are energy independent for incident electron speeds that are much greater than the outer-orbital electron speeds. Then, if *w* is constant *W*=*w* [20]. Based on some experimental results for ion beams in noble and other gases [21], protocols assumed the same property for all the charged projectiles used in hadrontherapy (e.g., protons, helium and carbon ions) and established a unique *W*-value, regardless of the projectile property [18]. One of the goals of the present work, is to investigate if this hypothesis is correct.

Experimental *W*-values were measured mostly for electron impact on water vapor and other gases [22–24]. Regarding proton and heavy ion projectiles, there are a few experiments in gases [18]. Willens *et al.* [25] measured the *W*-values in vapor water for relatively low proton energies (10 MeV) compared with the ones currently used in hadrontherapy (250 MeV/u to 400 MeV/u). Measurements of this parameter in condensed media such as liquid water is a challenge. A procedure used for highly polar media is based on measuring the yield of chemical species produced by ionization [26]. For liquid water a value of 20,8 eV was obtained by measuring the yield of solvated electrons after electron irradiation [27,28]. The uncertainties in this *W*-value were not informed by the author, but we estimate that they could be considerable taking into account that the yield of solvated electrons represents a lower limit of the ionization yield.

In this context of scarce experiments and difficulties to obtain accurate results, particle transport simulations and theoretical models are necessary to calculate *W*-values. These calculations can be very complex, since all the inelastic primary particle cross sections and all the inelastic processes due to the cascade of secondary electrons must be included [18]. In a previous work, we applied the Fowler equation, based on the Continuous Slowing Down Approximation (CSDA), to calculate *W* and *w*-values for electron, proton and antiproton impinging on liquid and vapor water [13]. The results obtained were in good agreement with experimental data and other theoretical calculations. In this work, the differential *w*-values are calculated with the CSDA and with the new MDM-Ion MC code for ion impact on liquid water. Since hadrontherapy requires proton beams of energies up to 250 MeV and carbon ions beams up to 400 MeV/u, relativistic effects have to be included in the cross sections. In the next sections, we present a detailed description of the MDM-Ion code and the CSDA, including the inelastic collisions cross sections used for ion and electron transport in liquid water. Stopping power and *w*-values are compared with recommended data and with other theoretical results. The effects of consider direct multiple ionization and post-collisional Auger electron emission processes are investigated. The relevance of the electronic excitation cross sections used in *w*-values calculations is also analyzed. Finally, we discuss assumptions made in the current protocols on the independence of *w* and *W* values with regard to the incident particle energy and charge.

## 2. Methods

The stochastic nature of the interaction between particles and atoms or molecules of the media is well represented by MC codes. These particle transport codes allow to track the history of each particle, event-by-event, until a set threshold energy. To generate the trajectories of the incident and the other generated particles (i.e., secondary electrons produced by ionization processes), MC codes use random numbers to sample the different physical processes involved in the interactions. This requires the complete probability distribution functions for each physical process along with the cross sections (see section 2.3 for more details). For the sake of brevity, we summarize in this section the main assumptions of the MDM code with the new branch developed for ion impact, called MDM-Ion, and define the physical parameters involved in our study.

Another method to determine the physical parameters under study is the Continuous Slowing Down Approximation (CSDA), also described in this section. Unlike track-structure codes, this model considers that the particle loses energy continuously along its path as it traverses the medium. This model is widely used today to obtain different physical quantities of relevance in radiation dosimetry (ICRU, NIST).

## 2.1. MDM-Ion MC simulation

Particle track-structure simulation consists of a series of collisions (called events) separated by a free flight distance *d*. In a homogeneous medium and in absence of external forces, the step length of this flight distance follows the Poisson probability distribution characterized by the total mean free path $\lambda_T$ , that depends on the total cross section $\sigma_T$ and the molecular density of the medium *n* by the relation $1/\lambda_T = \sigma_T n$. $\sigma_T$ represents the sum of all the elastic and inelastic cross sections involved in the simulation for a projectile kinetic energy *T*.

The main assumptions underlying the ion-transport simulation MDM-Ion code are:

(a) The ion follows a straight-line trajectory (set as z direction). Indeed, ion-molecular elastic collisions are relevant for energies much lower than 0.3 MeV/amu [29].
(b) The kinetic energy of the ion is fixed as constant over the entire track length. Indeed, track lengths are chosen short enough so that a swift ion loses a small amount of its kinetic energy. The variation in the ion cross sections is considered negligible but the energy loss is computed to estimate stopping power or *w*-values.
(c) Electron capture processes are neglected for the high energies considered (above 10 MeV/u). Consequently, the charge states of protons and carbon ions are 1 and 6 respectively.
(d) Multiple ionization and post-collisional Auger electron emission after an inner molecular shell ionization are considered.
(e) Relativistic corrections on the projectile velocity were taking into account due to the high energy range studied, which goes from 10 MeV/u to 700 MeV/u.
(f) The energy loss results from inelastic collisions, i.e., ionization and electronic excitation processes.
(g) Electron ejection by incident ions is characterized by the same probability to be ejected in all the angles (isotropic distribution). In fact, the *w*-values and stopping power calculations are not influenced by their angular distribution.
(h) According to amorphous description, water molecules are distributed in a box with cubic geometry. Periodic boundary conditions [30] were applied to mimic particle equilibrium related to ejected delta electrons. The dimensions of the volume are set large enough to avoid any artificial correlation in the beam (z) direction due to periodical conditions.
(i) All electrons are followed up until their energy is below the threshold for electronic excitation, that is 8,4 eV.

Eventually, the code provides the coordinates of all the interaction events, as well as the type of collision along with the energy loss and the energy deposited at each interaction point for all particles (i.e., primary ion and secondary electrons). In Figure 1, the track structure of a proton and a carbon ion in liquid water are presented. The ions move in a straight line (set as positive z axis) with an energy of 10 MeV/u through the media. Each point along the ion path represents an inelastic interaction (such as an ionization or an electronic excitation) between the primary ion, and all the

secondary particles generated (electrons), with the media. Then, the spatial pattern of energy deposition at the microscopic level can be observed. The high density of inelastic events in the carbon ion trace in comparison with the proton projectile at the same velocity, is related to the dependence of inelastic cross sections with the square of the ion charge: when the cross sections are larger the mean free path is smaller. This allows us to observe more swift electron tracks moving far away from the core of the carbon ion path than in the proton case.

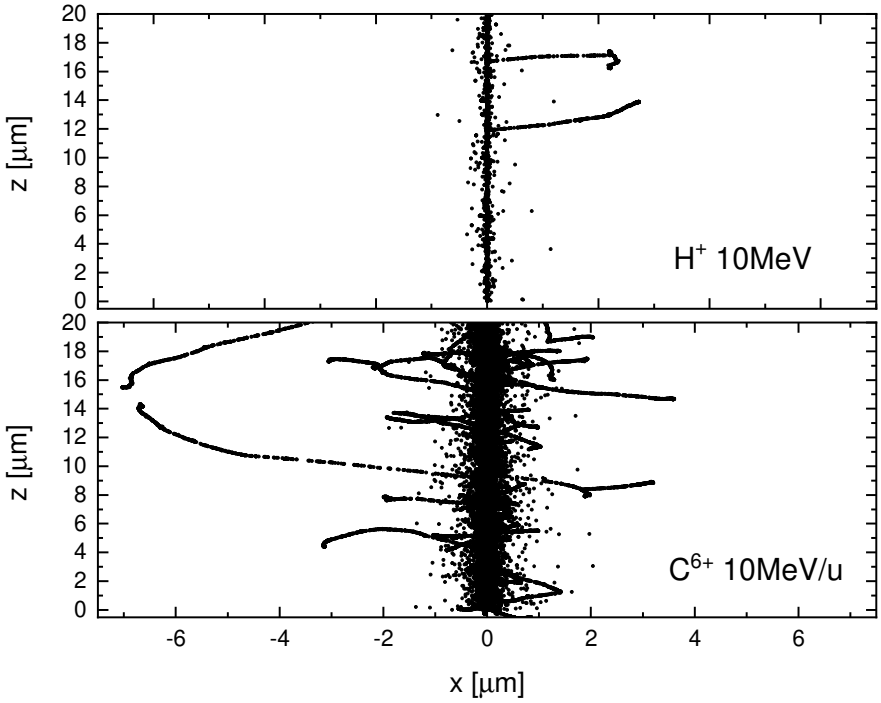


Figure 1: Track structure of proton and carbon ion in liquid water generated using MDM-Ion simulations, illustrating the spatial pattern of energy deposition at the microscopic level. The upper panel correspond to a 10 MeV proton and the panel below correspond to a 10 MeV/u carbon ion.

To calculate the differential *w*-values for each projectile ion energy, we calculated the ratio of the average total energy lost by the ion projectile, $E_{lost}$, and the average total number of electrons $N_{tot}$ created by ionizing water molecules inside the box. The ion length trace was set as 1 mm, z axis length, and the length of the other dimensions, x and y axis, are 3,0 mm. This was set according to the large range of the delta rays, especially for the high projectile energy. This number takes into account the ionizations generated by the ion projectile $N_{ion}$, and those generated by all the secondary electrons $N_e$. Therefore, the *w*-value can be expressed as:

$$w(T) = \frac{E_{lost}}{N_{tot}} \qquad \left[\frac{eV}{n°electrons}\right] \qquad (1)$$

where $N_{tot} = N_{ion} + N_e$.

Furthermore, by making the ratio between this average lost energy with the path length of the ion trace $Lz$ (positive z axis in our model) we obtain another parameter of interest, the Stopping power.

$$S(T) = \frac{E_{lost}}{Lz} \qquad \left[\frac{eV}{nm}\right] \tag{2}$$

By dividing it by the density of the medium (liquid water $\rho = 1g/cm^3$) we obtain the mass stopping power $S_{mass}$ in units of $MeVcm^2/g$. A mean value is calculated over a large set of tracks, large enough to obtain low fluctuations (Appendix C for more details).

## 2.2. The Continuous Slowing Down Approximation (CSDA)

To obtain the *w*-values for ion impact within the CSDA, we follow the expression from Dalgarno and Griffing (1958) [31]:

$$w(T) = \frac{\epsilon(T)}{\sigma_{ioniz}(T) + \sigma'_{ioniz}(T)} \tag{3}$$

where $\epsilon(T)$ is the stopping cross section, $\sigma_{ioniz}$ is the ionization cross section and $\sigma'_{ioniz}$ is the cross section associated with the production of an ion-electron pair by secondary processes.

The stopping cross section was calculated using the expression:

$$\epsilon(T) = \sum_n \sigma_n^{exc} E_n + \sum_k \left[ \int_0^{E_{max}} \frac{d\sigma_k^{ioniz}}{dE} (E + I_k)\, dE \right] \tag{4}$$

where $E_n$, and $E + I_k$ represents the energy transferred by the ion projectile during excitation and ionization processes. $E_n$ is the n-th excitation energy, $E$ is the ejected electron kinetic energy and $I_k$ is the *k*-th orbital binding energy. These values are listed in Appendix A. Since our study covers high-energy range, and as the electron capture process occurs at intermediate and low energies (less than 500 keV for proton impact and 6 MeV for carbon ions), this process was not considered in our calculations.

The cross section for secondary processes is given by:

$$\sigma'_{ioniz}(T) = \sum_k \left[ \int_0^{E_{max}} \frac{d\sigma_k^{ioniz}}{dE} N_e(E)\, dE \right] \tag{5}$$

where $d\sigma_k^{ioniz}/dE$ is the single differential ionization cross section for ion impact for each $k$-th molecular orbital as a function of the kinetic energy $E$ of the ejected electron. We multiply this value by $N_e(E)$, which is the average number of electrons generated by the full slowing down of an electron of energy $E$ produced in the ionization process of the medium by the ion. The $N_e(E)$ values used in the present work were obtained from the MDM code [13], see Figure 2.

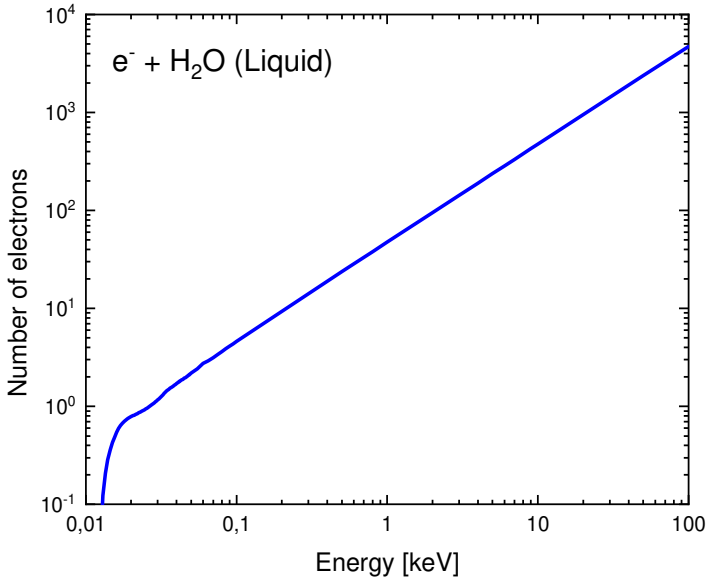


Figure 2: Number of electrons generated by electron impact on liquid water, as function of the projectile energy, calculated with the MDM code [13].

## 2.3. Inelastic cross section theory

The main inelastic processes considered in ion-matter interaction are ionization and electronic excitation. The effects of relativistic corrections on the projectile velocity applied to the cross sections are described in detail in this section. Multiple ionization and post-collisional effects are taken into account. Since not only the incident particle, but also all the secondary electrons produced by ionization processes must be followed, we describe in detail the cross sections used for ion and electron impact in liquid water.

### 2.3.1. Electron inelastic cross sections

**Ionization cross sections**

One of the most used models to calculate ionization cross section by electron impact is the Binary Encounter Bethe (BEB) semiempirical model [32]. This model is based on an adaptation of the Mott equation and accounts for electron impact on atomic and molecular targets. It has proven to be fairly accurate to describe the water molecule ionization in gas phase and it is not limited to the

high-energy domain like the First Born approximation. It provides both total and differential ionization cross sections for each energy level of the water molecule, as analytical functions with parameters obtained from fitting of experimental data. A complete description of the formulation used in the present work can be found in Gervais *et al.* (2006) [33], where some approximations were performed to a better description in the low energy range. Kim and Santos [34], made an extension of the BEB model to relativistic electron impact energies (RBEB). These relativistic cross sections, expressed in terms of the ratio between the electron speed and the speed of light in vacuum *c*, allow to calculate single differential ionization cross sections as a function of the ejected electron energy. For the sake of completeness, we give the expression of these cross sections in Appendix B.

Figure 3 shows the electron classical and relativistic kinetic energy as a function of the electron velocity normalized by the speed of light *c*. We can observe that relativistic kinetic energy differs from the classical result for electron energies beyond 20 keV.

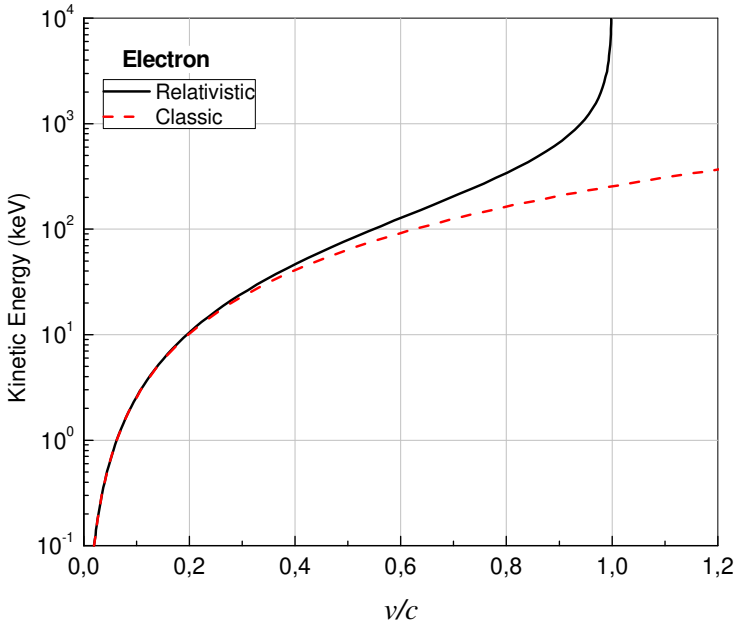


Figure 3: Electron kinetic energy calculated using the classical and the relativistic formulation, as function of electron velocity normalized by the speed of light in vacuum *c*.

A simple way to include relativistic effects in cross sections, avoiding complicated theoretical expressions, is to use an approximated expression for the projectile kinetic energy into the BEB model, as proposed by Plante and Cucinotta [35]. From the relativistic expression of the kinetic energy *T*, we obtain the projectile velocity *v*:

$$v = c\sqrt{1 - \frac{1}{(1 + T/m_0c)^2}} \tag{6}$$

and then, this value is used into the classical expression of the kinetic energy (for which the projectile mass is constant) to obtain

$$T^{RA} = \frac{1}{2} m_0 v^2 = \frac{1}{2} m_0 c^2 \left( 1 - \frac{1}{\left(1 + \frac{T}{m_0 c^2}\right)^2} \right) \tag{7}$$

where $T^{RA}$ is referred as a "relativist approximation (RA) to the kinetic energy".

In the case of an electron projectile, we use this new kinetic energy expression (7) to calculate the ionization cross section with the BEB model $\sigma_{BEB}(T^{RA})$, which will be named as BEB-RA, by replacing $m_0 c^2$ with $m_{0e} c^2$=0,511 MeV. This approximation allows to include relativistic effects into the cross sections used in the Monte Carlo, without changing the structure of the function.

Figure 4 (left) shows the ionization cross section for electron impact on liquid water calculated using the BEB, RBEB and BEB-RA models. We can observe a rise in the RBEB and BEB-RA curves from 20 keV onwards. The BEB-RA relativistic corrections allow a very good agreement with the RBEB results for energies up to 200 keV approximately. At higher energies the BEB-RA results underestimate those of RBEB.

**Excitation cross sections**

The relativistic approximation to the kinetic energy (RA) was also used to extend the electronic excitation cross sections already set in the MDM code [33]. It considers two electronic excitation states, $A^1B_1$ and $B^1A_1$ calculated with the semiempirical expression from Cobut *et al.* [36] (see analytical expression in Appendix A.2). Figure 4 (right) displays the total excitation cross section with and without relativistic correction, named as Cobut-RA and Cobut respectively.

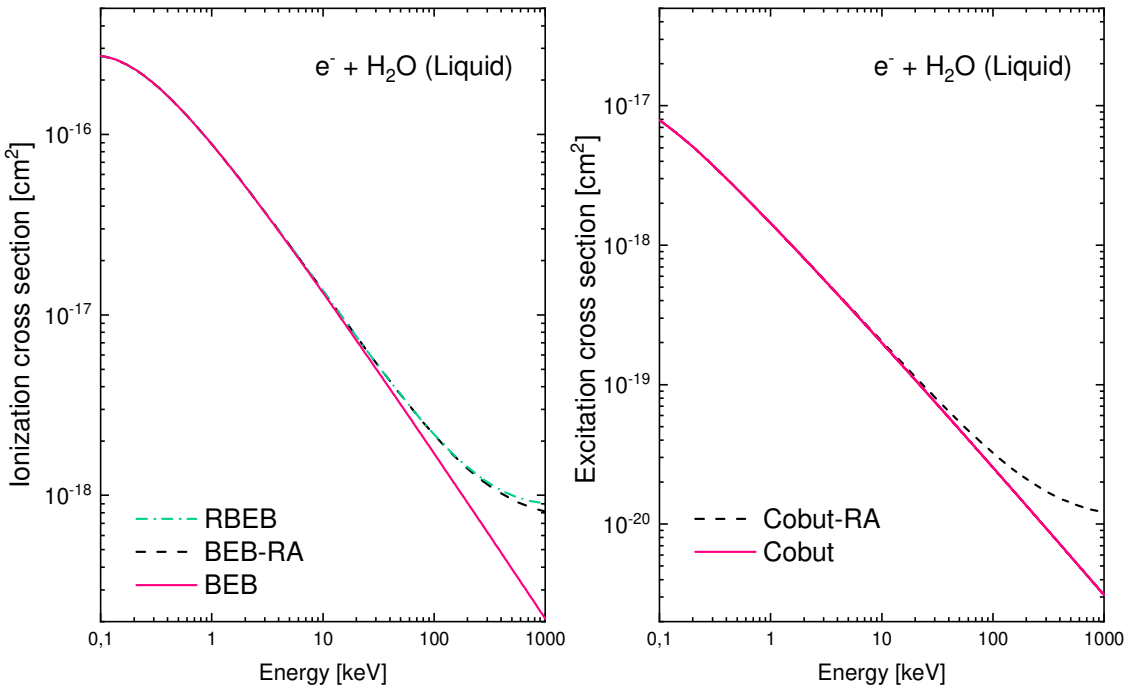


Figure 4: Ionization (left) and electronic excitation (right) cross sections for electron impact on liquid water. Ionization: BEB pink solid line, RBEB green dash-dotted line, BEB-RA black dashed line. Excitation: cross section from Cobut pink solid line, with relativistic correction Cobut-RA black dashed line.

Vibrational excitation cross sections are included as it was specified in the previous publication [13]. However, their contribution to the energy deposition is negligible.

As the present work is focused on the study of swift ion impact, it is very important to analyze the need to include (or not) relativistic corrections for electron-water interactions in MDM-Ion and CSDA calculations. To answer this question, in the next section we analyze the energy spectrum of the ejected electrons by swift proton and carbon ion impact on water molecules.

### 2.3.2. Ion inelastic cross sections

**Ionization cross sections**

The Single Differential Ionization Cross Section (SDICS) by proton impact on water is calculated using the semi-empirical equation developed by Rudd *et al.* [37]. This model, based on the First Born Approximation (FBA), gives an analytical representation of the differential cross sections over a wide range of proton energies. The analytical expression for the SDICS as a function of the ejected electron energy, has adjustable fitting parameters depending on the projectile velocity which were determined from experimental data and to satisfy FBA high energy asymptotic conditions. One of the advantages of this model is that it is very simple to implement in MC codes. Equation (7) shows the analytical expression, which depends only on the kinetic energy of the ejected electrons $E$, the electron binding energy and the projectile energy $T$:

$$\frac{d\sigma_k^{ioniz}(T,E)}{dE} = \frac{S}{I_k}\frac{(F_1 + F_2\, e)}{(1+e)^3}\left(\frac{1}{1+exp[\alpha(e-w_c)/v]}\right) \quad (7)$$

Here $I_k$ is the electron binding energy of the molecular $k$-shell with occupancy $N_k$, $e=E/I_k$ a scaled energy, $w_c = 4v^2 - 2v - R/4I_k$ is the scaled cutoff energy, with $v = \sqrt{T/I_k}$ a scaled velocity of the incident particle and $T$ is the kinetic energy of an electron with the same speed as the proton projectile with kinetic energy $T_p$, their relation is $T = (m_{0e}/m_{0p})T_p$ ($m_{0p}$ and $m_{0e}$ are the proton and electron mass at rest respectively). Furthermore, $S = 4\pi a_0^2 N_k R^2 / I_k^2$ with $a_0$ the Bohr radio and $R$=13,6 eV the Rydberg constant. The magnitudes $F_1(v)$, $F_2(v)$ and α are adjustment parameters; the first two are functions of $v$ and α is a dimensionless parameter near unity related to the size of the target. A detailed description of these quantities with their values, and the binding energies used in equation (7) are presented in Appendix A for liquid water.

In Figure 5, we show the ion velocity normalized to the speed of light in vacuum $c$ calculated as function of ion kinetic energy in MeV/u, using both the classic and the relativistic expressions for the ion projectile. As we can observe in this figure, the curves begin to separate at an energy of 50 MeV/u.

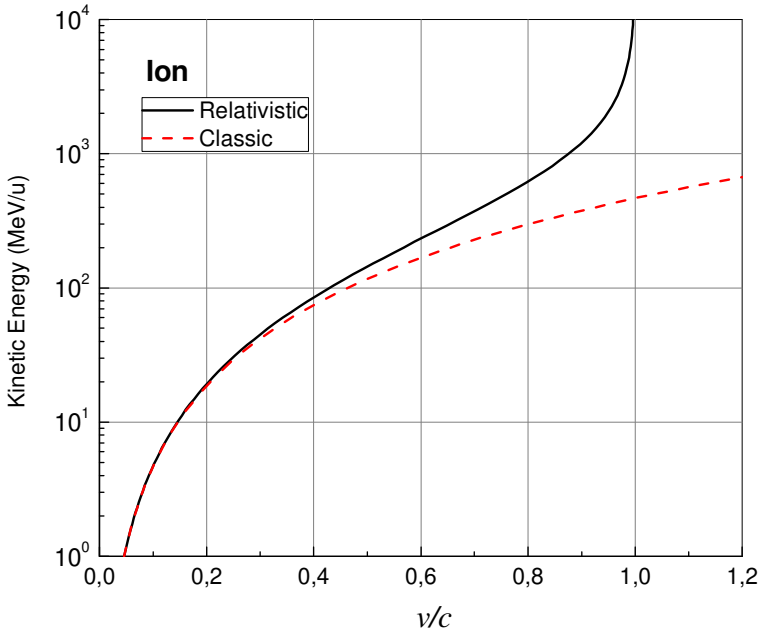


Figure 5: Ion kinetic energy calculated using the classical and the relativistic formulation as function of the particle velocity normalized by the speed of light in vacuum $c$.

Since the RA applied to the BEB model for electron impact gives very good results (section 2.3.1.) compared to a complete relativistic calculation, we decided to extend the same relativistic approximation to the case of ion-impact. To that end, we use expression (7), i.e., the relativist approximation to the kinetic energy $T^{RA}$, to calculate the cross sections. We can rewrite this

expression in function of the proton projectile energy $T_p$, keeping in mind that the electron has the same velocity as the proton projectile ($v = v_p$):

$$T^{RA} = \frac{1}{2} m_{0e} {v_p}^2 = \frac{1}{2} m_{0e} c^2 \left[ 1 - \frac{1}{\left( 1 + \frac{T_p}{m_{0p} c^2} \right)^2} \right] \tag{8}$$

where $m_{0p}c^2$ =938.26 MeV and $m_{0e}c^2$ =0.511 MeV.

The scaled velocity $v^2$ can now be rewritten as:

$$v^2 = T^{RA}/I_k = \frac{m_{0e} c^2}{2 I_k} \left[ 1 - \frac{1}{\left( 1 + \frac{T_p}{m_{0p} c^2} \right)^2} \right] \tag{9}$$

Thus, the single differential and total ionization cross section calculated with this relativistic correction, $d\sigma_{Rudd}(T^{RA}, E)/dE$ and $\sigma_{Rudd}(T^{RA})$, are referenced as Rudd-RA.

The FBA predicts that both excitation and ionization cross section are proportional to the square of the projectile charge $Zp^2$. In the high energy region, this approximation is valid and does not depend on projectile mass. At lower energies, however, more reliable theoretical models have to be used (i.e. CDW-EIS) [38]. In the present work, the ionization cross sections for swift carbon ions projectiles ($C^{6+}$) are obtained by multiplying the proton cross sections by $Zp^2$.

Figure 6 shows the total ionization cross section for proton and carbon ion impact on liquid water calculated with Rudd and Rudd-RA models. We can observe a rise in cross sections values for calculations with relativistic corrections compared with those that do not have it.

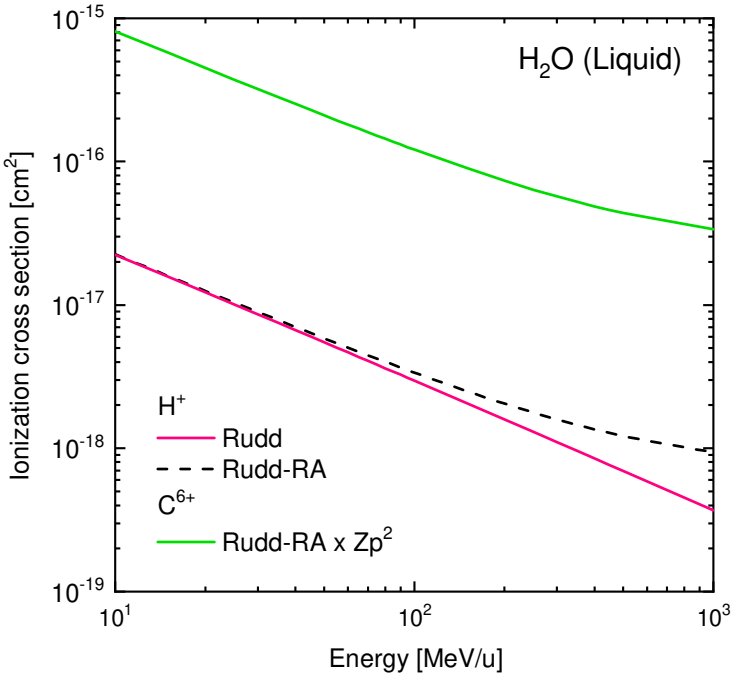


Figure 6: Total ionization cross sections by proton and carbon ion impact on liquid water. Rudd's model results using classical and relativistic velocities are compared.

The knowledge of SDICS allows us to study the energy spectrum of the emitted electrons, and consequently to determine whether it is necessary or not to include relativistic corrections in the cross sections for the interaction between the secondary electrons and the media. In Figure 7, we present four graphics of SDICS calculated with Rudd and Rudd-RA models as a function of the ejected electron energy by proton impact on liquid water. The proton impact energies shown are 1, 10, 100 and 400 MeV. Relativistic effects show up in the graphics of 100 and 400 MeV proton impact energies, where the curves begin to diverge. We found that for high impact energies, the probability of generating an electron with kinetic energy greater than 10 keV was smaller than 0.1%, and the average energy of the emitted electrons is ~ 45 eV. We also observed that incorporating relativistic cross sections for ionization and excitation processes by electron impact do not change the total number of ion pairs generated by the collisions. Therefore, considering that the scope of the present work is to study the w-values, and for the sake of simplicity, the inelastic interactions between the ejected electrons and the media are represented by the non-relativistic cross sections [33]. However, for the study of micro-dosimetry and biological effects, the relativistic cross sections for secondary electrons should be considered, as proposed by Plante and Cucinotta [14].

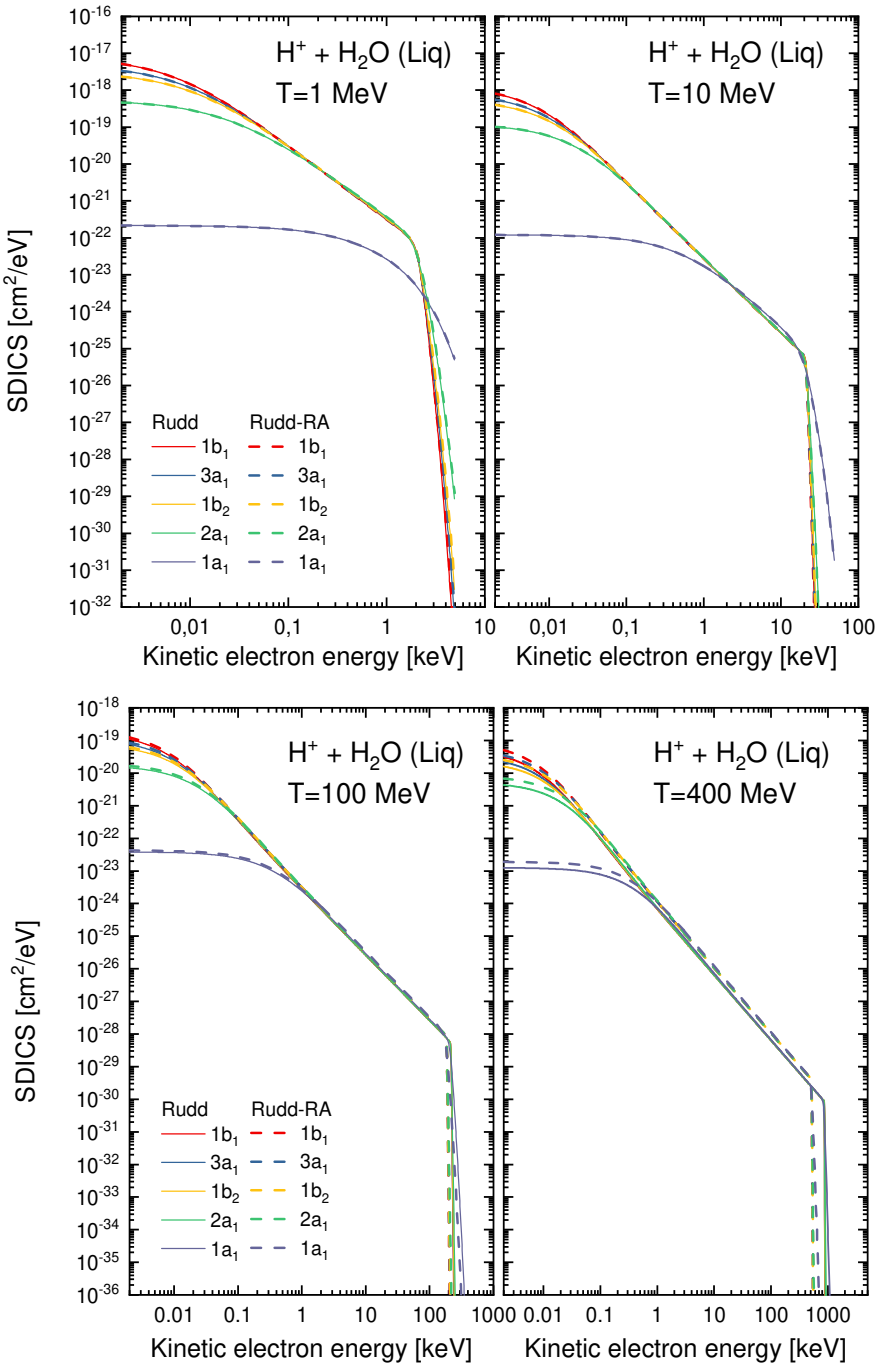


Figure 7: Ionization SDICS by proton of 1, 10, 100 and 400 MeV kinetic energies using the Rudd´s model with and without relativistic approximation on the projectile velocity.

**Multiple ionization and Post-collisional Auger electron emission**

Multiple ionization processes produced by the impact of fast ions on atoms and molecules have been a matter of active research during the last decades [33,39,40]. These processes are commonly divided into two mechanisms: the direct single and multiple ionization and the post-collisional electron emission. In the first one, the direct interaction between the projectile and the target produce the ejection to the continuum of one or more electrons. As a consequence, the residual target remains in a highly excited state with vacancies in the shells. When the projectile is assumed to be far away,

the second mechanism occurs. The vacancies created in the inner shells by ionization are filled by electrons from the outer shells. During these transitions, energy is released as photon emission or is absorbed to produce autoionization of the molecule through Auger-type emission. This post-collisional effect can occur between intershell Auger and/or intrashell Coster-Kronig electron ionization, depending on the shell from which the electron was ejected, and the shell from which the electron transitioned to fill the vacancy. In our study, only the Auger-type electron emission following after one or two core electrons ionization was included, since they are the dominant multiple ionization processes at high impact energies [39]. The influence of this Auger electron emission to the differential *w*-value was studied in detail. Due to the transition between the electrons in the molecular orbitals, the Auger electron have a specific well-defined kinetic energy. In our calculations it was considered that an Auger emission occur (with a probability of 100%) when an electron from the core shell $1a_1$ is ionized by the impact of an ion or electron projectile during a single or double ionization process. Then, deexcitation of an electron from the upper level $2a_1$ moves to the vacancy and an electron is emitted from the same level. Therefore, the kinetic Auger electron energy is set to 17,46 au or 475,08 eV. The summary of the transition probabilities is presented in the Evaluated Atomic Data Library (EADL) [41] atomic database for oxygen atom.

**Excitation cross sections**

The impact of the excitation cross sections used in the codes on the physical parameters calculated was analyzed in detail. There are only few experiments of electronic excitation cross sections for water molecules measured by photo absorption [42], but none for proton impact. Semiempirical models developed for electron impact [36,43] are based on these experiments, and show significant differences in the cross sections values. In the case of proton impact, the cross sections are commonly obtained by scaling the electron cross sections, based on the FBA velocity dependence, i.e., $\sigma_{exc}^{proton}(T_p) = \sigma_{exc}^{electron}(T)$, where the kinetic energies for proton impact $T_p$ and electron impact $T$ are related by $T = (m_{0e}/m_{0p})T_p$.

In this uncertain context, we scaled two semiempirical models developed for electron impact, to obtain the proton electronic excitation cross section: the Green and Stolarski (GS) [44] and the Cobut [36] models. For both models, the same electronic excitation states were taken into account ($A^1B_1$ and $B^1A_1$). Additionally, three other states were included in one model (Ryd A+B; Ryd C+D and Diffuse band) to show the impact on the physical parameters studied (see Appendix A for details). Relativistic corrections to the ion velocity (called RA) were also included, as it was made for the ionization cross section. The Green and Stolarski model is referred as GS or as GS-RA when relativistic corrections are included. The Cobut model, already used in the MDM code for electron

impact (see section 2.3.1) is referred as Cobut or as Cobut-RA. In this work, plasmon excitation was not included since collective excitations will decay mainly by ionization of water molecule [33].

In Figure 8, the electronic excitation cross sections for liquid water with and without relativistic corrections of these two models are compared. Observing the curves for the same two excitation states ($A^1B_1$ and $B^1A_1$) for both models, we observe a large difference between them, reaching almost an order of magnitude for high energies. The difference is even larger when comparing with the one that considers five electronic states. Another important point to mention is the relationship of these excitation cross sections with the ionization cross section, especially the ratio between them.

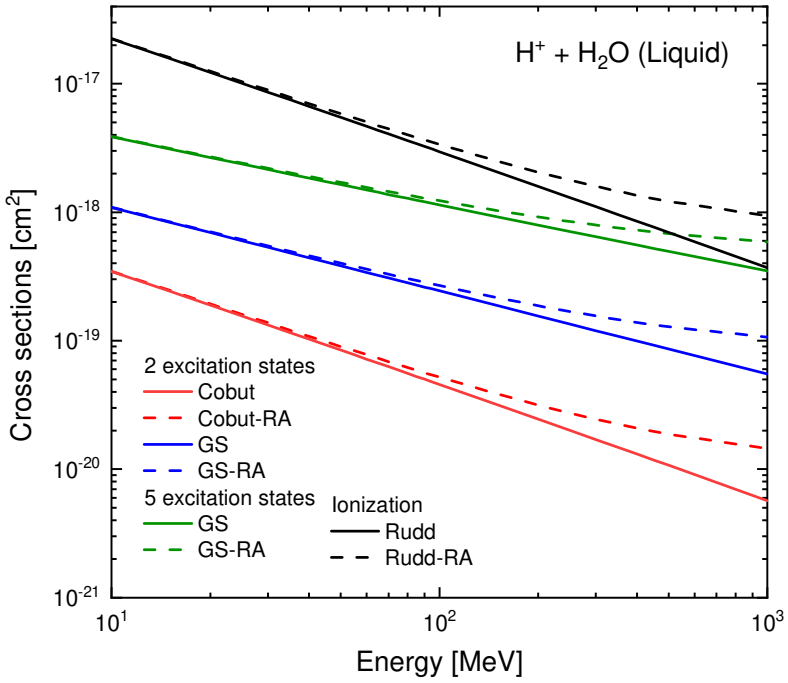


Figure 8: Electronic excitation cross section for proton impact on liquid water using two different models, GS and Cobut and different excitation levels in the GS model. They are compared with the ionization cross section from the Rudd model. Relativistic corrections are shown in the curves referred as RA.

As we can observe, the difference between the Rudd-RA and the Cobut-RA curves remains almost constant across the whole energy range. If we compare the Rudd-RA with the GS-RA curves, with two or five states, the difference gets smaller going towards higher energies. Observing the curves without the relativistic correction is more obvious and a cross between the ionization (Rudd) and the excitation (GS five states) cross sections take place for high energies. This relationship between ionization an excitation has a strong impact on the *w*-values as it will be presented in the next section of results.

# 3. Results

## 3.1. Ion Stopping Power

The mass stopping power ($S_{mass}$) for proton and carbon ion impact on liquid water are presented in figures 9 and 10. The MDM-Ion simulation and the CSDA approximation are compared with recommended data and measurements. Our calculated values represent the total mass electronic stopping power considering the ionization and the electronic excitation processes with two excited states ($A^1B_1$ and $B^1A_1$).

In Figure 9, we compare $S_{mass}$ calculated with the CSDA and MDM-Ion codes using the same inelastic cross sections, i.e., Rudd model for ionization and Cobut model for electronic excitation. A good agreement is observed between them, and with both experimental values [45,46] and recommended data from NIST and ICRU 49 [47,48]. As expected, we observe a relativistic effect beyond 50 MeV. It is important to mention that the values from NIST have an estimated uncertainty from 1% to 4% in the high-energy region [48] and the experimental data an uncertainty around 5%. Calculations on the MDM-Ion were run to reach statistical uncertainties lower than 1% (see Appendix C for more statistics details of these calculations).

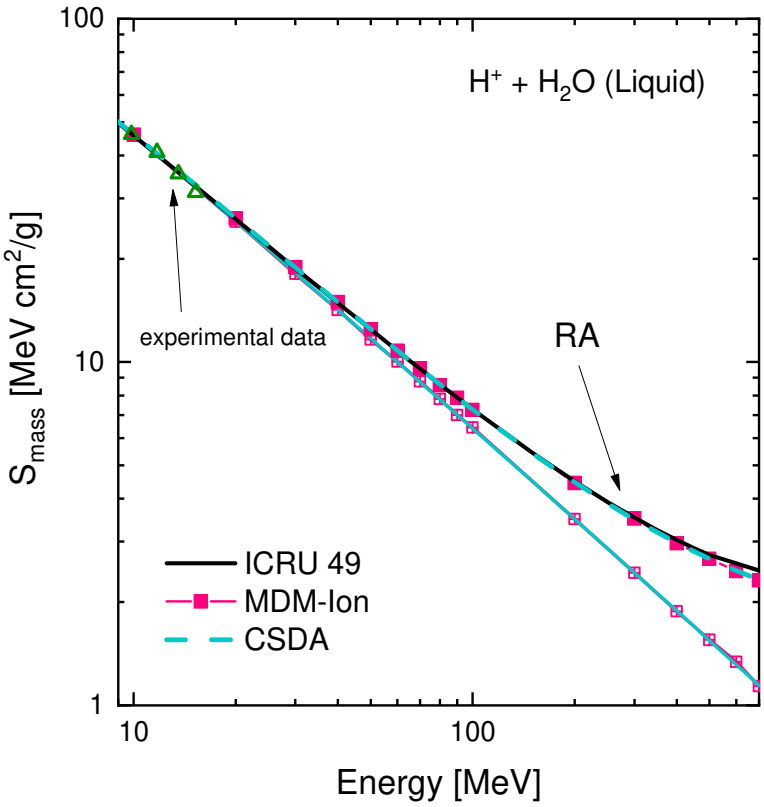


Figure 9: Comparison of the mass stopping power in liquid water for proton impact calculated with the CSDA formalism (dash line and solid line with no relativistic approximation) and the MDM-Ion in liquid water (square+line and open square+line with no relativistic approximation). They are also compared with

recommended data from ICRU 49 (solid balck line) and experimental data from Siiskonen *et al.* 2011 [46]. (triangles).

Figure 10 shows the $S_{mass}$ for carbon ion projectiles. Each method matches very well with the other one and with the recommended values from ICRU 73 [49] on the range of high relativistic energies. Values from the MDM-Ion have a statistical uncertainty smaller than 1%, while those of ICRU 73 can reach higher uncertainties, from 4% onwards.

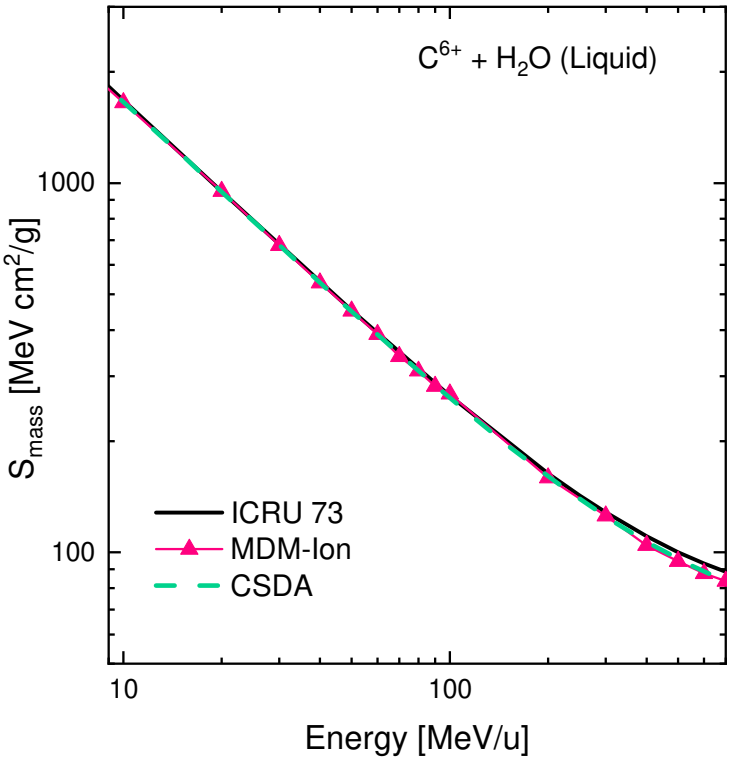


Figure 10: Carbon ion mass stopping power in liquid water calculated using the CSDA formalism and the MC MDM-Ion model. They are compared with recommended data from ICRU 73 [49].

To test the inelastic cross sections introduced for ion impact, the $S_{mass}$ was also calculated using the two semi-empirical models of excitation cross sections described in section 2.3.2. We will refer as model 1 the one that considers the excitation cross sections of Cobut, and model 2 the one that considers the GS cross sections. The results, presented in Figure 11, show good agreement between them and also with recommended data.

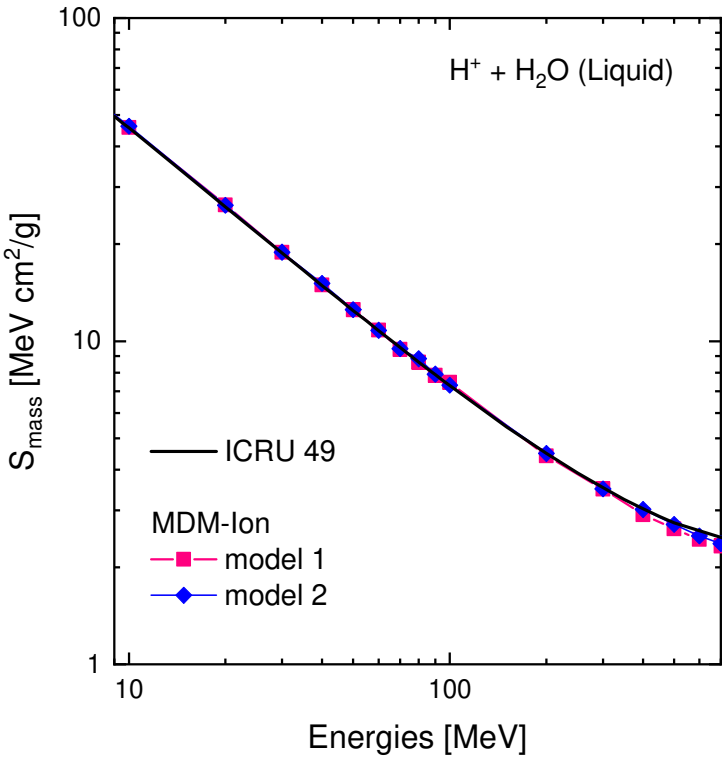


Figure 11: Comparison of the mass stopping power for proton impact implementing two models in the MDM-Ion calculations. Model 1: Rudd-RA and Cobut-RA cross sections; Model 2 Rudd-RA and GS-RA. They are also compared with recommended data of ICRU 49 [48].

In Figure 12, we present the relative percentage difference between the computed MDM-Ion and CSDA mass Stopping Power with the ICRU recommended values. As we can observe, for both projectiles the discrepancy is less than 2% for energies below 100 MeV/u. Beyond this energy the percentage of discrepancy increases, due to the relativistic approximation made in the cross sections. The curves including MDM-Ion calculations present deviations associated to statistical fluctuations.

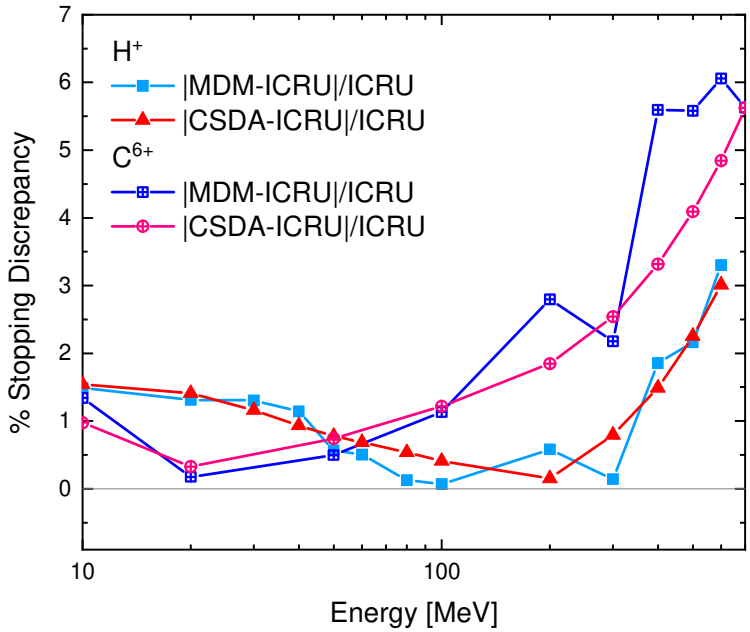


Figure 12: Relative percentage difference between the MDM-Ion and CSDA mass Stopping Power calculated data with the ICRU recommended values.

## 3.2. Differential w-values

The differential *w*-values were calculated by applying the CSDA and the MC code MDM-Ion for the transport of proton and carbon ion projectiles. In this section we present the results by taking into account relativistic corrections on the projectile velocity and multiple electron emission. We also show the relevance of the excitation cross sections used in the calculation of the *w*-values.

### 3.2.1. Excitation cross section dependence

Differential *w*-values for proton and carbon ion impact on liquid water were calculated using the MDM-Ion code. In Figure 13, *w*-values calculated using the Cobut and GS models are compared (no relativistic correction and post-collisional effects are taken into account yet). It can be observed an almost constant behavior with Cobut model. In the case of GS model, it is observed a higher *w*-value when we consider the same two electronic excitation states as the Cobut model, that increases by considering five excitation states.

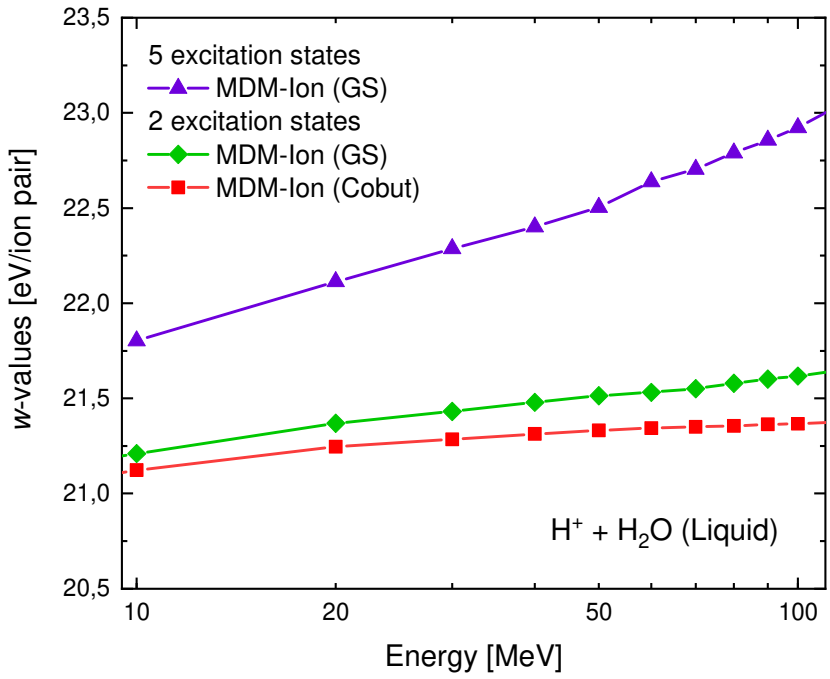


Figure 13: Differential *w*-values calculated with MDM-Ion for proton impact on liquid water, calculated with different excitation cross section models and different number of electronic states. Ionization CS were calculated with Rudd model. square+line represents Cobut cross sections; diamond+line represents GS cross sections, in both cases considering two electronic excitation states. triangle+line represents GS cross sections with 5 electronic excitation states.

In the following MDM-Ion calculations, the Cobut electronic excitation cross sections model is used to be in accordance with the model introduced for electron transport into the MDM code.

### 3.2.2. Relativistic Approximations (RA) in cross sections

Figure 14 shows the *w*-values for swift proton impact on liquid water calculated with the CSDA and the MDM-Ion code, introducing RA in ionization and excitation cross sections. The MDM-Ion results with and without RA are compared. The error bars in these values represent a 99.7 percent confidence interval (see Appendix C for details in the statistics used). For energies higher than 50 MeV it can be observed that the values with and without relativistic corrections differ by less than 0,5% contrary to the results shown for the stopping power (see previous section 3.1).

Comparing the *w*-values with RA calculated with CSDA and MDM-Ion, we can observe a very good agreement between them. A small difference can be appreciated beyond 100 MeV which could be attributed to an overestimation of the number of electron-ion pairs in the CSDA calculations. This method is very sensitive to small fluctuations in the calculation and require a large data base.

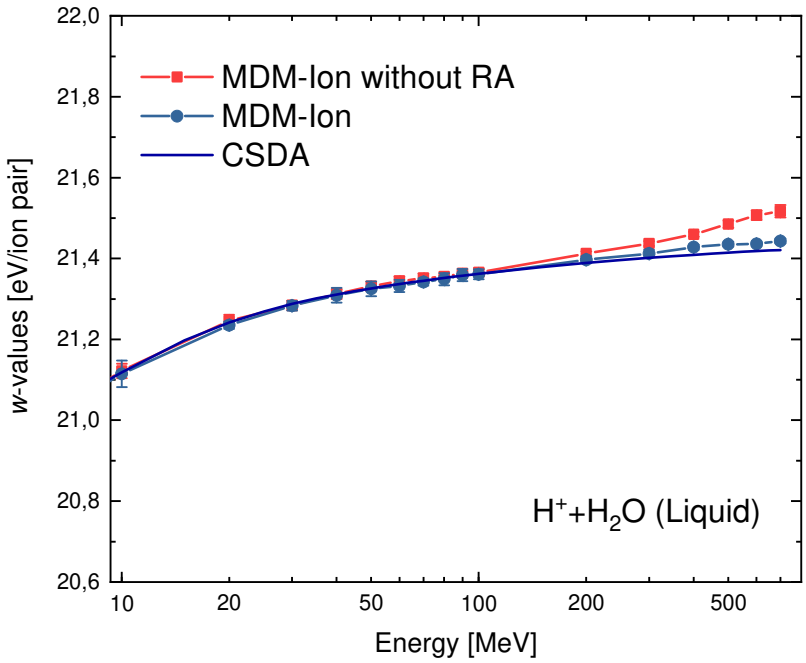


Figure 14: Differential *w*-values for proton impact on liquid water with and without relativistic corrections in the projectile velocity calculated with MDM-Ion and the CSDA.

### 3.2.3. Multiple ionization and electron Auger emission

To study the influence of Auger electron emission on the differential *w*-values for ion impact, it is essential to study first its effects on the integral *W*-values for electron projectiles. In Figure 15 we present the *W*-values calculated with the MDM code for electron impact on liquid water. We observe differences in *W*-values depending on whether Auger electrons emission is considered. The discrepancy between these curves can reach 4% for an electron energy of 10 keV. The relativistic effect was not considered in these calculations since it has not relevance for energies lower than 20 keV.

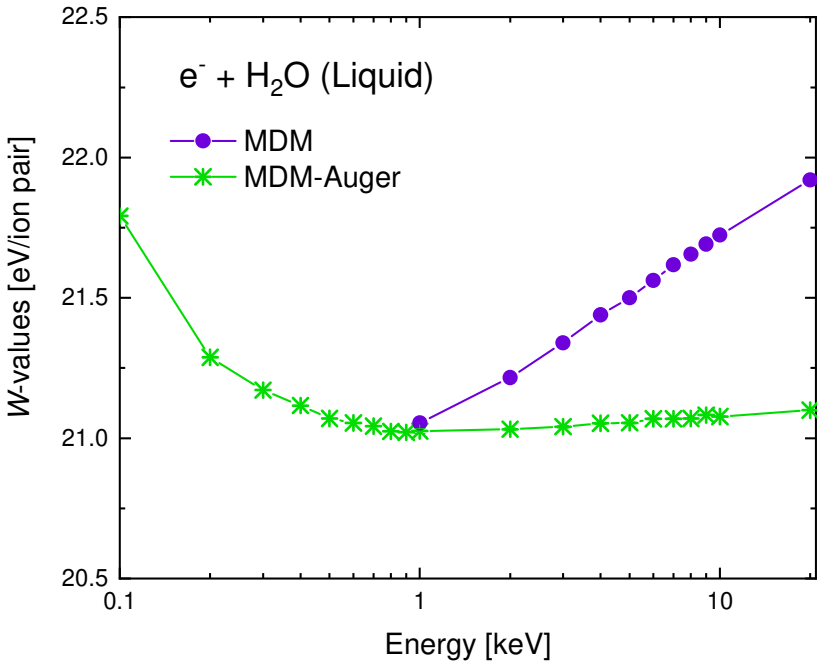


Figure 15: *W*-values for electron impact on liquid water with and without Auger electron emission calculated with the MDM code.

Figure 16 shows the differential *w*-values with and without Auger electrons for swift proton and carbon ions projectiles. The curves for both projectiles coincide for this high energy range. This is related to the dependence of the ionization and excitation cross sections with the square of the projectile charge $Zp^2$ at high impact energy. At medium and low energies, the electronic capture and ion charge exchange processes starts dominating over the electronic excitation and ionization processes. Such observations were also made for the mass stopping power, in figures 9 and 10 presented in the previous section. The study of the *w*-values in this low energy region is an interesting topic in dosimetry research because it is the region where the ion deposits its maximum energy in the medium, called the Bragg peak, and will be the subject of further research.

It can be observed that the *w*-values considering Auger emission are smaller than without them. For high-energy impact, Auger emission dominates the multiple ionization cross sections as was observed for the case of Ne and other atomic targets [39]. A mean value of 20,6 eV is marked with a straight line considering the Auger electrons with an uncertainty corresponding to 1%.

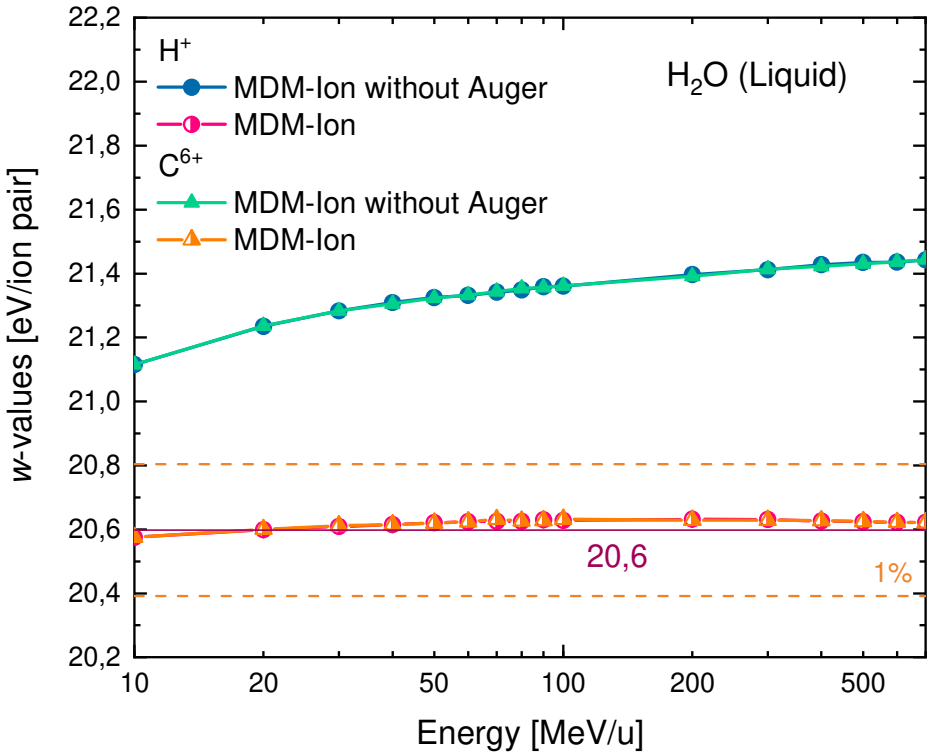


Figure 16: Differential *w*-values for proton and carbon ion impact on liquid water with relativistic corrections in the projectile velocity. Auger electron emission was also taking into account.

We also made calculations with or without considering the direct double ionization process, but since it has relevance only at lower energies it did not influence the *w*-values results.

In Figure 17, MDM-Ion results are compared with other MC codes and with CSDA calculations performed by other authors for proton and electron impact. The *w*-values, calculated using the MDM-Ion code, reach an asymptotic value of ~20,6 eV. Baek and Grooswendt (2007) [50] calculated the integral and differential *w*-values for proton impact on liquid water using an analytical expression based on the CSDA. To do so, they determined the ratio between the ionization cross section and the stopping power values from ICRU. To calculate the single differential ionization cross sections they used three different models, one from Dingfelder *et al.* (2000) [51], one from Emfietzoglou *et al.* (2000) [29] and the HKS (Hansen-Kocbach–Stolterfoht) model [52]. The *w*-values obtained lies between 21,5 eV and 26,5 eV in the energy range of 1 MeV to 10 MeV, and display an increase with increasing energies.

In Figure 17 we also compare our calculations from MDM with other MC codes for electron impact [15]. To include in the same figure electron and proton projectiles, we scaled the electron projectile energy to plot the integral *W*-value as a function of the proton kinetic energy with the same velocity as the electron projectile. Above 1 MeV, all the curves become relatively flat but with different values. The MDM code reaches a constant value of 21,1 eV which has a good agreement with the experimental 20,8 eV value. This value has been determined indirectly from measurements

of the radiolytic yield of solvated electrons [26]. It is also very close to that obtained for proton and carbon ion projectiles. The codes PARTRAC [3] and RETRACK [14] give higher values than that obtained from MDM, reaching 25,5 eV and 22,8 eV respectively. The inelastic cross sections included in the PARTRAC code are based on a non-relativistic first-order plane-wave Born approximation and a model of the dielectric response function of liquid water. It takes into account the five electronic excitation states presented in this paper with the GS model (see Appendix A). Auger electron emission after the $1a_1$ orbital ionization was also included. The RETRACK code uses the Rudd's formalism for the ionization cross sections and the Cobut model for electronic excitation states $A^1B_1$ and $B^1A_1$, but adding the plasmon excitation that increases considerably the total excitation cross section. This code also includes electron-parent ion recombination, autoionization and molecular fragmentation post-collisional processes.

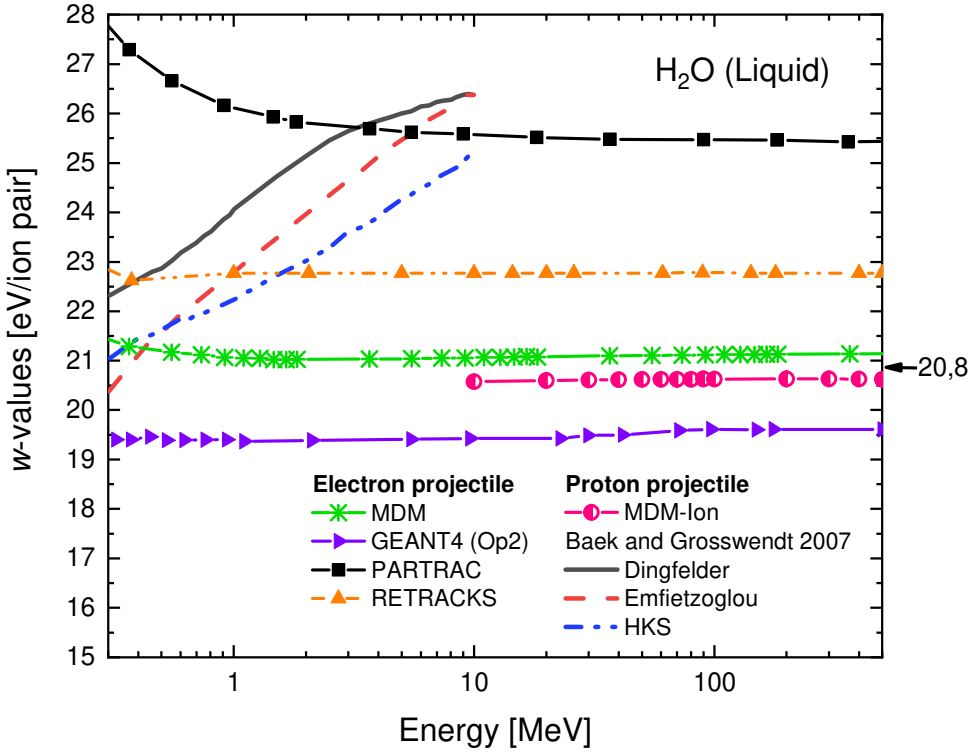


Figure 17: Differential *w*-values for proton impact are compared with electron impact *W*-values (integral) for different MC codes and CSDA on liquid water. Electron projectile: MDM (green star), GEANT4_Op2 (purple row), PARTRAC (black square) and RETRACKS (orange triangle). Proton projectile: MDM-Ion (half pink circle), CSDA with different models (lines red, blue and black). The value from indirect measurements of 20,8 eV is indicated by an arrow.

Geant4-DNA results, calculated with one of the options of inelastic cross sections available, are also shown in Figure 17. The "option 2" constructor (referred as Geant4_Op2 in the figure) includes the Auger electron emission process and takes an energy of cut-off for the tracking of 7,4 eV, obtaining a constant *W*-value of 19,5 eV [15]. Another option (Geant4_Op4) [53] gives the same asymptotic value as the RETRACKS code.

## 4. Discussion

The $S_{mass}$ for swift proton and carbon ion impact on liquid water calculated with the two methods, MDM-Ion and CSDA, are in very good agreement with experimental and with recommended data. The results for the high energies considered do not show a strong dependence on the excitation cross sections used because the energy deposition is dominated by the ionization processes. Instead, the *w*-values show to be very sensitive to the choice of the excitation cross section models as well as the number of excitation states considered. As can be observed in Figure 13, *w*-values calculated with the Cobut model have a constant behavior for all the projectile energies, as it was observed in experimental results for other atomic and molecular targets [54]. This is related to the almost equal trend between the ionization and the excitation cross sections (e.g. a constant ratio between the cross sections) according to the FBA, as proposed by Fano [55]. This asymptotic behavior does not occur if we use the GS excitation cross sections. We also observe an important increase in the *w*-values when using the 5 electronic excitations levels. This is related to a lower probability to produce ionizations when the proportion of excitations is increased, thus generating a lower number of electron-ion pairs. Therefore, *w*-values have a strong dependence on the magnitudes of the ionization and excitation cross sections and on the ratio between them: the larger this ratio is, the smaller the *w*-value.

Regarding the relativistic approximation made on the projectile velocities, we can observe that the *w*-values calculated with and without this correction have a very small difference between them. This behavior was expected, since the ratio between ionization and excitation cross sections is not affected by the relativistic approximation. On the contrary, this correction has a strong impact on the stopping power results since it has a direct relation with the cross section and no with the ratio between them (see figures 9 and 10).

The Auger emission post-collisional effect was included for electron, proton and carbon ion impact. The relevance of including this effect for high energy impact was observed for all the projectiles studied (see figures 15 and 16 for electron and ion impact respectively). As it was expected, the *w*-values considering Auger electrons is smaller than without them because the number of electrons produced by the projectile increases without losing any extra energy in this post-collisional effect.

The dependence with the projectile charge was also investigated. The *w*-values for carbon ions match with the proton curve. This independence with the ion charge occurs because, at the high energies studied, both the ionization and excitation cross sections have a dependence with the square

of the projectile charge $Zp^2$ and then the ionization and excitation cross sections ratio does not change. In figure 17, *w*-values for electron and proton impact on liquid water calculated with MDM and MDM-Ion codes are also in very good agreement with each other and with the only one experimental value existing according our knowledge. These results agree with the conclusions of Christophorou about the characteristics of *w*-values for other media [56]: this parameter is insensitive not only to the incident particle energy (at high impact energies) but is also nearly independent of the radiation quality. The insensitivity of *W* to the particle energy means that the measurement of ionization is equivalent to the measurement of relative energy loss determinations. Then, the Bragg curve (that is the number of ions created per unit path length) has the same shape than the energy-loss curve [26]. These results are relevant in radiation dosimetry and are the bases of reference dosimetry in hadrontherapy. Results from PARTRAC, RETRACKS and Geant4-DNA MC codes, show asymptotic behaviors of this parameter as function of the incident electron energy. The observed differences in the *w*-values are related to the excitation cross sections used and to the post-collisional processes considered, showing the relevance of calculate this physical parameter as a benchmark for MC codes developed for radiobiological research. Geant4-DNA option 2 constructor (that introduce the default models for the cross sections) gives the best agreement with our MDM and MDM-Ion calculations. Results from Baek and Grosswendt [50], obtained applying a very simple approximations based on the CSDA, shown an increasing trend with proton energy that does not agree with the MC results nor with the expected projectile energy independence.

To summarize, across the entire energy range studied, an agreement within a 2% is achieved for MDM-Ion and MDM with the measured value of 20,8 eV. Regarding the other MC codes, the discrepancy between them and our MDM results reaches up to 7%, related to the choice of the inelastic processes cross sections, especially for the case of electronic excitation and post-collisional effects.

## 5. Conclusions

In this work we presented the Monte Carlo code MDM-Ion developed to calculate physical parameters of fundamental interest in hadron therapy: the stopping power and the *w*-values for swift proton and light ion impact on liquid water. We investigated the impact of the excitation cross sections, the relativistic corrections in the ion velocity and the post-collisional Auger emission in the physical parameters studied. Stopping power are strongly dependent on the ionization cross sections and then, the relativistic corrections are mandatory at impact energies greater than 50 MeV/u. MDM-Ion and CSDA results are in excellent agreement with recommended data.

The *w*-values were found to be very sensitive to the choice of the inelastic cross sections, especially on the excitation cross-sections where semi-empirical models differ from each other even though they are based on the same experimental data. We also showed the relevance of including multiple electron emission for the high energies used for hadrontherapy treatments. We obtained a 4% of difference by considering or not the post-collisional Auger electrons emission. Results obtained with the MDM-Ion for proton and carbon ions are in very good agreement with the MDM results for electron impact and have constant behaviors across the high energy range investigated. Numerical calculations based on the CSDA (using the same inelastic cross sections) are also in good agreement with the MDM and MDM-Ion results. These calculated *w*-values are in good agreement with the 20,8 eV value derived by indirect measurements for electron impact on liquid water. In addition, our results are close and have the same behavior as other simulation codes widely used today for radiation dosimetry and radiobiological research.

According to the results obtained, we can conclude that *w*-values are independent of the projectile charge (light ions), mass and energy at the high energy regime. Research at intermediate and low energies is required to better understand the behavior of *w*-values and its dependence with the projectile charge and mass. However, more experimental *w*-values are needed for liquid water to be used as a benchmark (together with the stopping power) for MC codes developed for nano and micro-dosimetry.

In future work, the MDM-Ion code will be extended to calculate stopping power and *w*-values in air and in other media of interest in hadron therapy.

**Declarations of interest: none**

## Acknowledgements

This work was partially supported by the following institutions: Consejo Nacional de Investigaciones Cientificas y Tecnicas (CONICET), Universidad Nacional de Rosario (UNR) (PID-ING 515 and AVEdocente), LABEX PRIMES (ANR-11-LABX-0063) of Université de Lyon, within the program 'Investissementsd'Avenir' (ANR-11-IDEX-0007) operated by the French National Research Agency (ANR). We also acknowledge the financial support by ITMO Cancer in the framework of Plan Cancer 2009-2013.

## Appendix A. Theoretical proton cross sections

### A.1. Ionization cross section

The differential ionization cross section was calculated using the semi-empirical equation developed by Rudd *et al* (1992) [37] for proton impact on molecular targets. The analytical expression in function of the kinetic ejected electron energy *E* is,

$$\frac{d\sigma_k^{Rudd}(T,E)}{dE} = \frac{S}{I_k}\frac{(F_1 + F_2\, e)}{(1+e)^3}\left(\frac{1}{1+exp[\alpha(e-w_c)/v]}\right) \quad \text{(A. 1)}$$

where $I_k$ is the binding energy of the electron in the k shell with occupancy $N_k$, $e=E/I_k$, $w_c= 4v^2-2v-R/4I_k$, with $v= (T/I_k)^{1/2}$ the projectile velocity and $T$ is the kinetic energy of an electron with the same speed as the projectile. $S=4\pi a_0^2 N_k R^2/I_k^2$ with $a_0$ the Bohr radio and R=13,6 eV the Rydberg constant. The magnitudes $F_1(v)$, $F_2(v)$ y α are adjustment parameters; the first two are associated with the primary particle by the following expressions and their values are shown in table

$$\begin{aligned} F_1 &= L_1 + H_1 \\ F_2 &= L_2\, H_2/(L_2 + H_2) \\ H_1 &= A_1\, ln(1 + v^2)/(v^2 + B_1/v^2) \\ L_1 &= C_1\, v^{D1}/[1 + E_1 v^{(D1+4)}] \\ H_2 &= A_2/v^2 + B_2/v^4 \\ L_2 &= C_2\, v^{D2} \end{aligned} \quad \text{(A. 2)}$$

Table 1: Molecular orbital, binding energy and mean kinetic energy used to calculate single ionization on liquid water taken from Dingfelder [51].

| Molecule | Molecular orbital | $I_k$ | $N_k$ |
|---|---|---|---|
| $H_2O$ liquid | $1a_1$ | 539.0 | 2 |
| | $2a_1$ | 32.30 | 2 |
| | $1b_2$ | 16.05 | 2 |
| | $3a_1$ | 13.39 | 2 |
| | $1b_1$ | 10.79 | 2 |

Table 2: Parameters used to calculate single ionization on liquid water from Dingfelder [51].

| Parameters | $H_2O$ liquid | Internal orbitals |
|---|---|---|
| $A_1$ | 1.02 | 1.25 |
| $B_1$ | 82 | 0.50 |
| $C_1$ | 0.45 | 1.00 |
| $D_1$ | -0.8 | 1.00 |
| $E_1$ | 0.38 | 3.0 |
| $A_2$ | 1.07 | 1.10 |
| $B_2$ | 14.6 | 1.30 |
| $C_2$ | 0.6 | 1.00 |
| $D_2$ | 0.04 | 0.0 |
| $\alpha$ | 0.064 | 0.66 |

### A.2. Excitation cross section

Green and Stolarski's semi-empirical model [44] gives and analytical expression for total electronic excitation cross sections for electron impact. In this model, the cross sections for each excited state k are defined by:

$$\sigma_k^{GS}(T) = \frac{Aq_0}{E_k^2}\left(\frac{E_k}{T}\right)^{\omega}\left[1-\left(\frac{E_k}{T}\right)^{\gamma}\right]^{\nu} \qquad [cm^2] \tag{A.3}$$

$T$ being the kinetic energy of the electron, the energy of the k-th excited state $E_k$, $q_0 = 4\pi a_0^2 R^2 = 6.51410^{-14}\ [eV^2cm^2]$ $A, \omega, \gamma$ and $\nu$ adjustment parameters (see Table 3 below).

Table 3: Parameters used to calculate excitation cross section on liquid water taken from Kutcher and Green [43].

| Molecule | Excited state | $E_k$ | $A$ | ω | $\nu$ | γ |
|---|---|---|---|---|---|---|
| $H_2O$ liquid | $A^1B_1$ | 8.4 | 0.0302 | 0.6537 | 3.0 | 1.561 |
| | $B^1A_1$ | 10.10 | 0.0617 | 0.6447 | 3.0 | 1.537 |
| | *Rydberg A+B* | 11.26 | 0.0142 | 0.6670 | 3.0 | 1.415 |
| | *Rydberg C+D* | 11.93 | 0.0590 | 0.5796 | 3.0 | 1.813 |
| | *Diffuse band* | 14.10 | 0.086 | 0.4535 | 3.0 | 3.0 |

Following the work of Cobut *et al.* (1998) [36] and Kim (2001) [57] to scale the energy dependence deduced from the Born approximation, the differential cross section for electron impact has the form:

$$\frac{d\sigma_k^{Cobut}}{dW} = \frac{\pi f_{0k}}{(T+W+A)} e^{-\alpha_k (W-W_{0k})^2} ln\left(\frac{q_{max}}{q_{min}}\right) \tag{A.4}$$

where $T$ is the kinetic electron energy, $W$ an excitation energy, A=8.6 eV is the ionization energy threshold, $W_{0k}$ is the mean excitation energy for the considered level, $\alpha_k$ defines the energy spread around $W_{0k}$, and $f_{0k}$ is the oscillator strength for the transition. $q_{max}$ and $q_{min}$ are the maximum and minimum energy transfers respectively in function of $t = T/W$,

$$\begin{gathered} q_{min} = 2t - 1 - 2\sqrt{1-1/t}\,, \\ q_{max} = 2t - 1 + 2\sqrt{1-1/t} \quad if\ q_{max} < 1 \\ q_{max} = 1 \quad if\ \ q_{max} \geq 1 \end{gathered} \tag{A.5}$$

| Excited states | $W_{0k}$ *(eV)* | $\alpha_k$ *(eV$^{-2}$)* | $f_{0k}$ |
|---|---|---|---|
| $A^1B_1$ | 8.4 | 3 | 0.0187 |
| $B^1A_1$ | 10.10 | 1 | 0.0157 |

To obtain the cross sections for proton impact the electron kinetic energy is scaled to the proton energy $T_p$ by $T = m_{0e}/m_{0p}T_p$; $\sigma_{exc}^{proton}(T_p) = \sigma_{exc}^{electron}(T)$.

## Appendix B. Theoretical electron cross sections

B.1. Ionization cross section

Single differential cross section was formulated by Kim and Rudd [32]:

$$\frac{d\sigma_k^{BEB}(e,t)}{dE} = \frac{S}{I_k\,(t+u+1)}\left[\frac{-1}{t+1}\left(\frac{1}{(e+1)}+\frac{1}{(t-e)}\right)\right. \\ + \left(\frac{1}{(e+1)^2}+\frac{1}{(t-e)^2}\right) \\ \left. + ln\,t\left(\frac{1}{(e+1)^3}+\frac{1}{(t-e)^3}\right)\right] \quad [cm^2/eV] \tag{B.1}$$

where $I_k$ is the binding energy , $U_k$ is the kinetic energy of the media of the binding electron, $N_k$ is the number of occupancy in the k shell, $t = T/I_k$, $e = E/I_k$, $u = U_k/I_k$, $S = 4\pi a_0^2 N_k R^2/I_k^2$, $a_0 = 0.5292\,10^{-8}$ cm Bohr radio and $R = 13.61\,eV$ is the Rydberg energy.

Table 4: Molecular orbital, binding energy from Dingfelder et al. (1998) [58] and mean kinetic energy from Rudd et. *al* (1992) [37] on liquid water.

| Molecule | Molecular Orbital | $I_k$ | $U_k$ | $N_k$ |
|---|---|---|---|---|
| $H_2O$ | $1a_1$ | 540.0 | 794.75 | 2 |
| | $2a_1$ | 33.30 | 71.0 | 2 |
| | $1b_2$ | 16.60 | 48.695 | 2 |
| | $3a_1$ | 14.70 | 59.2 | 2 |
| | $1b_1$ | 11.95 | 61.45 | 2 |

The extension to the relativistic energies was developed by Kim, Santos and Parente (2000) [34]. This expression is in function of the ratio between the electron velocity and the speed of light c,

$$\beta_t^2 = v_t/c, \quad \beta_t^2 = 1 - \frac{1}{(1+t')^2}, \quad t' = T/m_0c^2 \\ \beta_b^2 = v_b/c, \quad \beta_b^2 = 1 - \frac{1}{(1+b')^2}, \quad b' = I_k/m_0c^2 \\ \beta_u^2 = v_u/c, \quad \beta_u^2 = 1 - \frac{1}{(1+u')^2}, \quad u' = U_k/m_0c^2 \tag{B.2}$$

where $v_t$, $v_b$ and $v_u$ are the velocity of an electron with kinetic energy $T$, $I_k$ and $U_k$ respectively. $m_0$ is the electron mass in rest.

Therefore, the relativistic equation of single differential cross section is

$$\frac{d\sigma_k^{RBEB}}{dE}(e,t) = \frac{4\pi a_0^2 \alpha^4 N_k}{(\beta_t^2+\beta_b^2+\beta_u^2)2b'I_k}\left[\frac{-1}{t+1}\left(\frac{1}{(e+1)}\right.\right.$$
$$\left. + \frac{1}{(t-e)}\right)\frac{1+2t'}{(1+t'/2)^2} + \frac{1}{(e+1)^2} + \frac{1}{(t-e)^2} + \frac{b'^2}{(1+t/2')^2} \quad \text{(B.3)}$$
$$\left. + \left(ln\left(\frac{\beta_t^2}{1-\beta_t^2}\right) - \beta_t^2 - ln(2b')\right)\left(\frac{1}{(e+1)^3} + \frac{1}{(t-e)^3}\right)\right]$$

where $\alpha = 1/137$ is the fine-structure constant.

Detailed explanations about the cross sections used in the present work to follow secondary electrons can be found in Gervais *et al.* 2006 [33].

## Appendix C. Uncertainties in the Monte Carlo calculations

To calculate the differential *w*-values and the Stopping Power we made several simulations in order to reach an uncertainty less than 1%. Since the number of simulations *N* was very big, we consider the uncertainty to be the standard deviation of the mean $\sigma_{mean}$ estimated as,

$$\sigma_{mean} = \frac{\sigma}{\sqrt{N}}$$

where $\sigma$ is an estimate for the standard deviation of the calculated quantity and N the number of simulations.

The percentage of the uncertainty was calculated by dividing this value with the mean of the magnitude in study, this is $\sigma_{mean}\% = \frac{Mean}{\sigma_{mean}} * 100\%$.

## References


[1] Nikjoo H, Uehara S, Emfietzoglou D, Cucinotta FA. Track-structure codes in radiation research. Radiat Meas 2006;41:1052–74. https://doi.org/10.1016/j.radmeas.2006.02.001.

[2] Plante I, Cucinotta FA. Energy deposition and relative frequency of hits of cylindrical nanovolume in medium irradiated by ions : Monte Carlo simulation of tracks structure. Radiat Env Biophys 2010;49:5–13. https://doi.org/10.1007/s00411-009-0255-7.

[3] Dingfelder M, Ritchie RH, Turner JE, Friedland W, Paretzke HG, Hamm RN. Comparisons of calculations with PARTRAC and NOREC: Transport of electrons in liquid water. Radiat Res 2008;169:584–94. https://doi.org/10.1667/RR1099.1.

[4] El Naqa I, Pater P, Seuntjens J. Monte Carlo role in radiobiological modelling of radiotherapy outcomes. Phys Med Biol 2012;57. https://doi.org/10.1088/0031-9155/57/11/R75.

[5] Monini C, Cunha M, Chollier L, Testa E, Beuve M. Determination of the Effective Local

Lethal Function for the NanOx Model. Radiat Res 2020;193. https://doi.org/10.1667/RR15463.1.

[6] Monini C, Cunha M, Testa E. Study of the Influence of NanOx Parameters. Cancers (Basel) 2018;10. https://doi.org/10.3390/cancers10040087.

[7] Cunha M, Monini C, Testa É, Beuve M. NanOx , a new model to predict cell survival in the context of particle therapy. Phys Med Biol 2017;62:1248–1268. https://doi.org/10.1088/1361-6560/aa54c9.

[8] Gervais B, Beuve M, Olivera GH, Galassi ME, Rivarola RD. Production of HO2 and O2 by multiple ionization in water radiolysis by swift carbon ions. Chem Phys Lett 2005;410:330–4. https://doi.org/10.1016/j.cplett.2005.05.057.

[9] Ouerdane H, Gervais B, Zhou H, Beuve M, Renault J-P. Radiolysis of Water Confined in Porous Silica : A Simulation Study of the Physicochemical Yields. J Chem Phys 2010;114:12667–74.

[10] Poignant F, Charfi H, Chan C-H, Dumont E, Loffreda D, Testa É, et al. Monte Carlo simulation of free radical production under keV photon irradiation of gold nanoparticle aqueous solution. Part I: Global primary chemical boost. Radiat Phys Chem 2020:108790. https://doi.org/10.1016/j.radphyschem.2020.108790.

[11] Poignant F, Ipatov A, Chakchir O, Lartaud P, Testa É, Gervais B. Theoretical derivation and benchmarking of cross sections for low-energy electron transport in gold. Eur Phys J Plus 2020;123:1–37. https://doi.org/10.1140/epjp/s13360-020-00354-3.

[12] Poignant F, Monini C, Testa É, Beuve M. Influence of gold nanoparticles embedded in water on nanodosimetry for keV photon irradiation ´ Floriane Poignant. Med Phys 2020. https://doi.org/10.1002/mp.14576.

[13] Tessaro VB, Poignant F, Gervais B, Beuve M, Galassi ME. Theoretical study of W-values for particle impact on water. Nucl Inst Methods Phys Res B 2019:1–7. https://doi.org/10.1016/j.nimb.2018.11.031.

[14] Plante I, Cucinotta FA. Cross sections for the interactions of 1 eV–100 MeV electrons in liquid water and application to Monte-Carlo simulation of HZE radiation tracks. New J Phys 2009;11. https://doi.org/10.1088/1367-2630/11/6/063047.

[15] Incerti S, Kyriakou I, Bernal MA, Bordage MC, Francis Z, Guatelli S, et al. Geant4-DNA example applications for track structure simulations in liquid water: A report from the Geant4-DNA Project. Med Phys 2018;45:e722–39. https://doi.org/10.1002/mp.13048.

[16] Nikjoo H, Emfietzoglou D, Liamsuwan T, Taleei R, Liljequist D, Uehara S. Radiation track, DNA damage and response - A review. Reports Prog Phys 2016;79:116601.

https://doi.org/10.1088/0034-4885/79/11/116601.

[17] Garcia-Molina R, Abril I, Heredia-Avalos S, Kyriakou I, Emfietzoglou D. A combined molecular dynamics and Monte Carlo simulation of the spatial distribution of energy deposition by proton beams in liquid water. Phys Med Biol 2011;56:6475–93. https://doi.org/10.1088/0031-9155/56/19/019.

[18] Andreo P, Burns DT, Hohlfeld K, Hu MS, Kanai T, Laitano F, et al. Absorbed Dose Determination in External Beam Radiotherapy: An International Code of Practice for Dosimetry based on Standards of Absorbed Dose to Water. IAEA TRS-398. Vienna; 2000.

[19] ICRU REPORT 78 - International Commission on Radiation Units and Measurements. Prescribing, Recording, and Reporting Proton-Beam Therapy. J ICRU 2007;7.

[20] ICRU REPORT 59 - International Commission on Radiation Units and Measurements. Clinical Proton Dosimetry Part I : Beam Production , Beam Delivery and Measurement of Absorbed Dose. 1998.

[21] Inokuti M, KrajcarBronić I, Srdoč D. Ch 8:Yields of ionization and excitation in irradiated matter. At. Mol. data Radiother. Radiat. Res. IAEA-TecDoc-799, 1995, p. 547–631.

[22] Combecher D. Measurement of w values of low-energy electrons in several gases. Radiat Res 1980;84:189–218. https://doi.org/10.2307/3575293.

[23] Christophorou LG, Blaunstein RP. Electron attachment in gases and liquids. Chem Phys Lett 1971;12:173–9. https://doi.org/10.1016/0009-2614(71)80643-7.

[24] ICRU REPORT 31 - International Commission on Radiation Units and Measurements. Average Energy Required To Produce An Ion Pair. 1979.

[25] Willems G, Baek WY, Grosswendt B. ENERGY DEPENDENCE OF W VALUES OF PROTONS IN WATER. Radiat Prot Dosimetry 2002;99:347–50.

[26] Mozumder A. Chapter 4: Ionization and Excitation Phenomena. Fundam. Radiat. Chem., 1999.

[27] Jonah CD, Matheson MS, Mille JR, Hart EJ. Yield and decay of the hydrated electron from 100 ps to 3 ns. J Chem Phys 1976;80:1267–70.

[28] Sumiyoshi T, Tsugarau K, Yamada T, Katayama M. Yield of Solvated Electrons at 30 Picoseconds in Water and Alcohols. Bull Chem Soc Jpn 1985;58:3073–5.

[29] Emfietzoglou D, Papamichael G, Kostarelos K, Moscovitch M. A Monte Carlo track structure code for electrons (~10 eV-10 keV) and protons (~0.3-10 MeV) in water: Partitioning of energy and collision events. Phys Med Biol 2000;45:3171–94. https://doi.org/10.1088/0031-9155/45/11/305.

[30] Cunha M, Testa E, Beuve M, Balosso J, Chaikh A. Considerations on the miniaturization of detectors for in vivo dosimetry in radiotherapy: A Monte Carlo study. Nucl Instruments

Methods Phys Res Sect B Beam Interact with Mater Atoms 2017;399:20–7. https://doi.org/10.1016/j.nimb.2017.03.078.

[31] Dalgarno A, Griffing GW. Energy per ion pair for electron and proton beams in atomic hydrogen. Proc R Soc London Ser A Math Phys Sci 1958;248:415–28. https://doi.org/10.1098/rspa.1958.0253.

[32] Kim YK, Rudd ME. Binary-encounter-dipole model for electron-impact ionization. Phys Rev A 1994;50:3954–67. https://doi.org/10.1103/PhysRevA.50.3954.

[33] Gervais B, Beuve M, Olivera GH, Galassi ME. Numerical simulation of multiple ionization and high LET effects in liquid water radiolysis. Radiat Phys Chem 2006;75:493–513. https://doi.org/10.1016/j.radphyschem.2005.09.015.

[34] Kim YK, Santos JP, Parente F. Extension of the binary-encounter-dipole model to relativistic incident electrons. Phys Rev A - At Mol Opt Phys 2000;62:052710–1. https://doi.org/10.1103/PhysRevA.62.052710.

[35] Plante I, Cucinotta FA. Ionization and excitation cross sections for the interaction of HZE particles in liquid water and application to Monte Carlo simulation of radiation tracks. New J Phys 2008;10. https://doi.org/10.1088/1367-2630/10/12/125020.

[36] Cobut V, Frongillo Y, Patau JP, Goulet T, Fraser MJ, Jay-Gerin JP. Monte Carlo Simulation of Fast Electron and. Radiat Phys Chem 1998;51:229–43.

[37] Rudd ME, Kim YK, Madison DH, Gay TJ. Electron production in proton collisions with atoms and molecules: Energy distributions. Rev Mod Phys 1992;64:441–90. https://doi.org/10.1103/RevModPhys.64.441.

[38] Galassi ME, Rivarola RD, Beuve M, Olivera GH, Fainstein PD. Theoretical calculation of single ionization in collisions between protons and low-[Formula Presented] molecules at intermediate and high energies. Phys Rev A - At Mol Opt Phys 2000;62:6. https://doi.org/10.1103/PhysRevA.62.022701.

[39] Galassi ME, Rivarola RD, Fainstein PD. Multiple electron emission from noble gases colliding with proton beams, including postcollisional effects. Phys Rev A - At Mol Opt Phys 2007;75:1–7. https://doi.org/10.1103/PhysRevA.75.052708.

[40] Rivarola RD, Galassi ME, Fainstein PD, Championc C. Computation of Distorted Wave Cross Sections for High-Energy Inelastic Collisions of Heavy Ions with Water Molecules. Adv. Quantum Chem. Theory heavy ions Collis. Phys. Hadron Ther., 2013, p. 231–63.

[41] Perkins T, Cullen DE, Chen MH, Hubbell JH, Rathkopf J, Scofied J. Tables and Graphs of Atomic Subsh , ell and Relaxation Data Derived from the LLNL Evaluated Atomic Data Library (EADL), Z=1 - 100. vol. 30. 1991.

[42] Heller JM, Hamm RN, Birkhoff RD, Painter LR. Collective oscillation in liquid water. J Chem Phys 1974;60:3474–82. https://doi.org/10.1063/1.1681563.

[43] Kutcher GJ, Green AES. A model for energy deposition in liquid water. Radiat Res 1976;67:408–25. https://doi.org/10.2307/3574338.

[44] Green AES, Stolarski RS. Analytic models of electron impact excitation cross sections. J Atmos Terr Phys 1972;34:1703–17.

[45] Shimizu M, Kaneda M, Hayakawa T, Tsuchida H, Itoh A. Nuclear Instruments and Methods in Physics Research B Stopping cross sections of liquid water for MeV energy protons. Nucl Inst Methods Phys Res B 2009;267:2667–70. https://doi.org/10.1016/j.nimb.2009.05.036.

[46] Siiskonen T, Kettunen H, Perajarvi K, Javanainen A, Rossi M, Trzaska WH, et al. Energy loss measurement of protons in liquid water. Phys Med Biol 2011;56:2367. https://doi.org/10.1088/0031-9155/56/8/003.

[47] NIST. National Institute of Standards and Technology n.d. http://www.nist.gov/pml/data/ionization/.

[48] ICRU REPORT 49 - International Commission on Radiation Units and Measurements. Stopping Powers and Ranges for Protons and Alpha Particles. 2015.

[49] ICRU REPORT 73 - International Commission on Radiation Units and Measurements. Stoping of Ions Heavier Than Helium. J ICRU 2005;5. https://doi.org/10.1093/jicru/ndi001.

[50] Baek WY, Grosswendt B. W values of protons in liquid water. Radiat Prot Dosimetry 2007;126:93–6. https://doi.org/10.1093/rpd/ncm019.

[51] Dingfelder M, Inokuti M, Paretzke HG. Inelastic-collision cross sections of liquid water for interactions of energetic protons. Radiat Phys Chem 2000;59:255–75. https://doi.org/10.1016/S0969-806X(00)00263-2.

[52] ICRU REPORT 55 - International Commission on Radiation Units and Measurements. Secondary Electron Spectra from Charged Particle Interactions. 1996.

[53] Kyriakou I, Incerti S, Francis Z. Technical note: Improvements in geant 4 energy-loss model and the effect on low-energy electron transport in liquid water. Med Phys 2015;42:3870–6. https://doi.org/10.1118/1.4921613.

[54] Stolterfoht N, DuBois RD, Rivarola RD. Electron emission in heavy ion-atom collisions, Springer Series on Atoms and Plasmas. 1997.

[55] Fano U. On the theory of ionization yield of radiations in different substances. Phys Rev 1946;70:44–52. https://doi.org/10.1103/PhysRev.70.44.

[56] Christophorou LG, Anderson VE, Birks JB. ATOMIC AND MOLECULAR RADIATION PHYSICS. London: n.d.

[57] Kim Y. Scaling of plane-wave Born cross sections for electron-impact excitation of neutral atoms. Phys Rev A 2001;64:1–10. https://doi.org/10.1103/PhysRevA.64.032713.

[58] Dingfelder M, Hantke D, Inokuti M, Paretzke HG. Electron inelastic-scattering cross sections in liquid water. Radiat Phys Chem 1998;53:1–18. https://doi.org/10.1016/S0969-806X(97)00317-4.